The 5th European sCO2 Conference for Energy Systems
March 14-16, 2023, Prague, Czech Republic

2023-sCO2.eu-121

PERFORMANCE COMPARISON OF TEMPERATURE SENSORS FOR CLOSED CYCLES OPERATING WITH SUPERCRITICAL CO_2

Pierre Belleoud*
Cranfield University
Bedfordshire, United-Kingdom
Email: pierre.belleoud@cranfield.ac.uk

Eduardo Anselmi Palma
Cranfield University
Bedfordshire, United-Kingdom

Jason Chetwynd-Chatwin
Rolls Royce plc
Bristol, United-Kingdom

Ioannis Roumeliotis
Cranfield University
Bedfordshire, United-Kingdom

ABSTRACT

Near the critical point of carbon dioxide (CO_2), small changes in temperature or pressure can result in large changes in the calculation of its thermodynamic properties, thus the right choice of instrumentation is of importance. This paper addresses the challenges related to CO_2 temperature measurement in small-diameter pipes and assesses different sensors utilizing Cranfield University's supercritical CO_2 test rig capabilities. In order to compare temperature sensor types for supercritical CO_2, a test tube has been designed to fit different sizes of temperature probes at the discharge of the transcritical compressors at the sCO_2 test rig. Different diameters of thermocouples (0.75 to 4.5 mm), Resistance Temperature Detectors (RTDs) and surface sensors were tested and compared in terms of amplitude and adaptability to sudden temperature changes. Results for different fluid conditions in the supercritical region of CO_2 were derived. The use of thermowell is discussed as it can offer a suitable compromise between practicality and 'internal' measurements. The results presented in this paper aim to provide a comparison of temperature sensors' performances for different regimes, transient or steady state.

Keywords: Instrumentation, Uncertainties, Thermocouples, Supercritical CO2, Transient.

INTRODUCTION

An accurate knowledge of the total temperature variation through turbomachinery is essential in quantifying its performance in understanding its operation and in applying efficient control. By measuring temperatures and pressures at various planes throughout a rotating machine, the performance of compressors and expanders may be calculated. This implies the selection of instruments being mounted on purposely designed supports and strategic positions. The selection of these instruments shall also address turbomachinery performance scenarios: steady-state or transient. The second scenario, measuring changing temperatures, is bounded by a specific concern: the sensor should ideally change its temperature at the same rate as the stream (or body) being measured. The relevance of this concern increases when considering the potential implications in control strategies for turbomachinery, specifically for closed cycles operating with supercritical CO_2. In the case of centrifugal compressors operating with this working fluid, on top of the classical challenges of avoiding surge, sits the ambition of keeping the inlet temperature within certain ranges near the critical point (7.4 MPa and 31 °C).

During the initial development of the test rig at Cranfield University in 2015, the available references of operative rigs were predominantly: Sandia National Laboratories [1], Naval Nuclear Integrated System Test [2] and Korea's rigs (by Korean Atomic Energy Research Institute [3], Korea Advanced Institute of Science and Technology and Korean Institute of Energy Research). These references plus paired conversations during the 1st European Seminar on SCO_2 Power Systems in 2016 [4], led to select RTDs Pt100 (± 0.2 °C for CO_2 stream) as temperature sensors for Cranfield's rig. However, as the rig commissioning progressed and more rigs started to report their operative results, see Table 1, it became a concern that for testing future turbomachinery, RTDs might not be the obvious selection for dynamic phenomena. On top of that, the location and mechanical features of the probes were also to be considered.

* corresponding author(s)

DOI: 10.17185/duepublico/77283

Table 1: Reported temperature sensors from test rig facilities used as references by Cranfield University

Facility	Temperature Measurement Technology	Device error (°C)	Temperature range investigated
SANDIA SNL [1]	RTD	± 1.1	Ambient to 811 K
KAPL / BAPL IST [5]	Thermocouple Type T (Special Limit of Error)	± 0.4	309 to 554 K
KAIST [3]	RTD	± 0.2	Ambient to 573 K
SCARLETT [6]	Thermocouple Type T RTD	± 0.1 ± 0.3	Ambient to 350 K
sCO2-HeRo [7]	Pt100	± 0.15	Up to 823 K
SUSEN [8]	Thermocouple Type K	± 0.5	Up to 823 K
Brunel [18]	RTD Type K	±0.03 to 0.06 ±1.5	223 to 523K 273 to 1273K
TU Wien [19]	RTD class AA RTD class A	0.1+0.0017T 0.15+0.002T	223 to 523K 173 to 723K

For example, Hexemer et al. [2] acknowledged the challenges for matching measurements against the pre-defined by the compressor manufacturer (Barber Nichols Inc) "total" compressor inlet conditions. Two different inlet flow areas (pipe and inlet compressor) needed to be considered when defining or measuring fluid conditions upstream of the compressor. The measured temperature and pressure should be "consistent" with the reference conditions stated in the compressor's map. Moreover, the preliminary transient results also demonstrated the importance of fast temperature monitoring of cooling water pre-cooler inlet temperature (ramped from 35 to 18 °C in 5 to 60 seconds) to keep compressor CO_2 temperature within ± 1 °F (± 1.8 °C) [2]. Later results provided by Clementoni in 2017 [9], confirmed that their rig sensors (thermocouples type T) were able to register small fluctuations of the compressor inlet temperature in the operations of up and down-power transient; specifically, 96 ± 1 °F (35.5 ± 1 °C) in windows of 50 seconds.

Similarly, on the topic of mechanical installation, Southwest Research Institute [10] previously pointed out the challenges of dynamic excitation of inserted thermocouples due to periodic vortex shedding. Suggesting performing FEA in thermowell design "to ensure sufficient separation between vortex shedding and mechanical natural frequencies and also that non-resonant probe stresses are well below the material's endurance limit operating temperatures" on p251 of [10]. Stuttgart [6] also disclosed their mechanical settings for estimating heat transfer and pressure drop near the critical point in a Ø 2 mm (inner diameter) copper tube. Including a discussion about the error impact of soldering their T-type thermocouples into milled channels on the surface of the test tube. More recently, SANDIA [11] exemplified the impact on transient measurement in the discharge of their Peregrine's turbine, due to improper insertion depth of their RTDs. Interestingly, the mechanical arrangement shown seemed simple but effective. Not much information has been found about the installation of Kiel-type probes, the use of exposed junction thermocouples or recommended types of shields for total temperature measurements in CO2 streams. Even, in 2021, the uncertainty assessment about instrumentation and measuring techniques for sCO2 compressors using ASME PTC-10 by Mortzheim [17]; indicated the use of T-type thermocouples inside custom-made thermowell configurations, which caused obstruction bigger than 30 % in the pipelines. A few more references, [18] and [19] can be found in Table 1 that complete this non-exhaustive list of sCO2 test facilities.

The right selection (and mechanical design) of temperature measurement for transient operation implies an iterative process of trial and error. At Cranfield University, it has been decided to inform the selection process for future turbomachinery with a series of experiences using the available test rig. A test tube and two measurement stations on the gas side of the rig have been monitored with different sensors to register and identify their time responses. This is relevant, as it seems that the selection of temperature sensors for monitoring closed cycles operating with supercritical CO2, will imply selecting two or three types of sensors, addressing primarily two challenges: accuracy and response time.

This paper will focus on relatively easy installations: surface, in-line tip insulated and thermowell; to create a measuring experience before attempting other approaches such as: bare exposed junction, grounded junction, radiation shield, or Kiel-type installation. After presenting the experimental setup and the condition of how the measurements were performed, this paper will discuss the different responses of the temperature sensors in terms of time response and in terms of value. A discussion on the impact of the sensor accuracy on the calculation of thermodynamic properties such as the density and the specific enthalpy will then be provided.

EXPERIMENTAL SETUP

The analysis conducted herein utilizes the Cranfield university sCO_2 test rig capabilities. This rig, shown in Figure 1, is composed of two 45 kW semi-hermetic compressors (1), one of which is regulated in frequency via an inverter, electronic expansion valves for high pressure (2a), liquid expansion (2c), flash gas (not shown), an industrial controller which regulates operating modes of compressors and fans (on/off, speed) and valve positioning (3), a liquid receiver of 60 L (4), a gas cooler of 200 kW (5) and a brazed plate heat exchanger of 95 kW (6). More details can be found in [12].

DOI: 10.17185/duepublico/77283

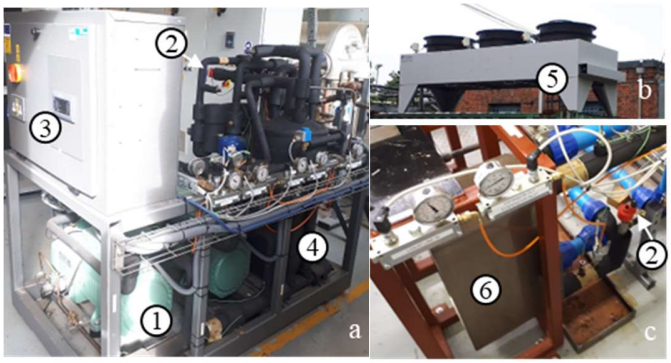

Figure 1: Cranfield supercritical CO_2 rig main components: compressors, liquid receiver and controller (a), gas cooler (b) and evaporator (c).

To compare the performance of different types of temperature sensors, a specifically designed test tube has been placed in parallel to the discharge of the compressor. This test tube includes a system of valves allowing isolation and depressurisation, which facilitates the replacement and inspection of the sensors. The testing section has been set in a straight run of the main discharge tube, away from 20 internal diameters of any elbows or t-pees, up and downstream, to avoid severe changes in flow direction that could modify the flow locally. The tube is equipped with two connections of 1/4" BSPP and one of 1/2" BSPP to be able to vary sensor sizes as shown in Figure 2. The test tube is made of a high-copper alloy that is 28.57 mm in outside diameter with a wall thickness of 1.78 mm (thermal conductivity of 260 $W.m^{-1}.K^{-1}$). A thermowell has been mounted on connection 1 and compression fittings have been placed on connections 2 and 3 to place the sensor element directly in the flow. Two sensors were placed at the surface of the tube. One of them is a K-type thermocouple of 0.75 mm placed on the surface of the tube with thermal paste and aluminium tape, see Figure 3, then covered with an additional layer of insulation foam of 13 mm of thickness and thermal conductivity of 0.033 $W.m^{-1}.K^{-1}$ at 0 °C. The second one is another K-type thermocouple designed to be installed on pipes. Due to its orientation and size, it was not insulated which will underline the effect of the natural convection within the laboratory room.

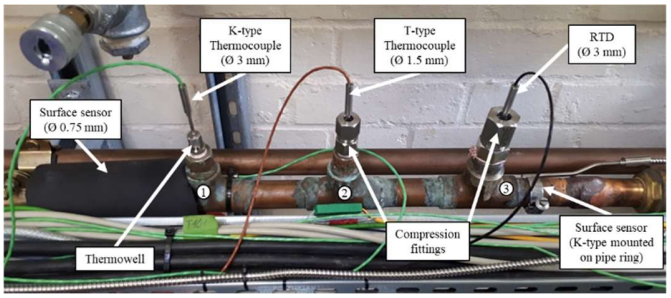

Figure 2: Test tube equipped with compression fittings, thermowell and temperature probes.

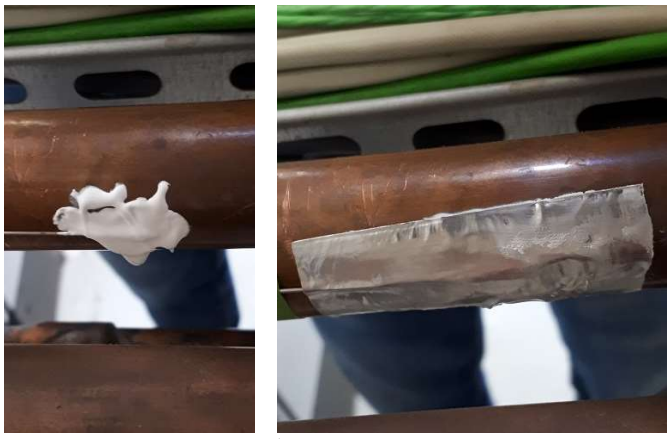

Figure 3: Installation of Ø 0.75 mm thermocouple at the surface of the pipe with a layer of thermal paste (right) and covered with aluminium tape (left).

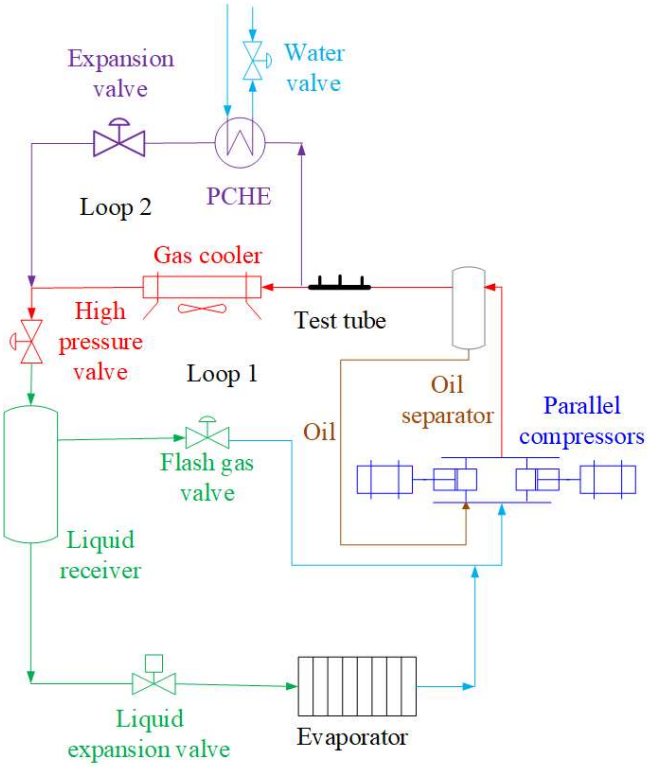

Figure 4: Diagram of the main experimental set-up and additional measurements.

TEMPERATURE PROBES

Different probes have been selected to be compared in this paper: RTD, K-type thermocouple and T-type thermocouple as a non-exhaustive list of common temperature probes in use. A summary of their characteristics is given in Table 2. When available, the manufacturer's typical time response is provided and compared against in-house tests in the same conditions. The

DOI: 10.17185/duepublico/77283

sensors were submitted to a step temperature change from the ambient (around 20 °C) to a boiling water bath at 100 °C. The time response given is the time to reach 63 % of the final temperature. The resulting dimensionless temperature for the five sensors, θ calculated via (1), has been plotted in Figure 5.

$$\theta = \left(\frac{T - T_{amb}}{T_{100\,°C} - T_{amb}}\right) \quad (1)$$

The response times thus measured have been added to Table 2. At first sight, measured values differ to some extent from the manufacturer's values which could be due to differences in the calibration protocol. However, the relative 'order' in the sensors is consistent, the RTD has the longest time response of 2.1 s and the thermocouples' time response is following the size of the sensor, the 0.75 mm in diameter has the fastest response and the 4.5 mm, the longest. These considerations can be useful when selecting the sensor as thin thermocouples may not support flow conditions (severe changes of flow momentum for instance) but if placed at the surface of the pipe, the lower the time response is, the better it is to compensate for the conduction through the pipes' wall.

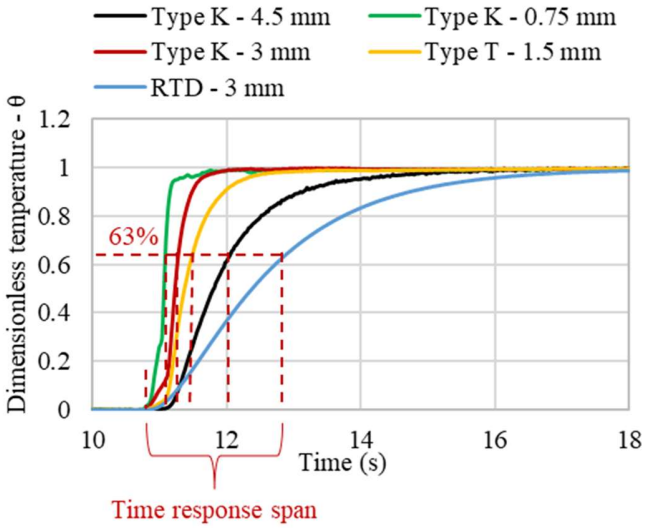

Figure 5: Step of temperature from ambient to 100°C.

To provide a theoretical value of the sensor time response within the test tube we can as well express the ratio (2), considering that the Biot Number, B_i, (3) is below one according to [19].

$$\frac{T - T_\infty}{T_i - T_\infty} = e^{-\frac{t}{\tau}} \quad (2)$$

$$B_i = \frac{h_{CO_2} L_{c_{sensor}}}{k_{sensor}} \quad (3)$$

The sensor used here has an insulated junction protected with a grade 316L stainless steel (SS) sheath filled with Magnesium Oxide (MgO). It is then possible to estimate the overall thermal conductivity (4), k_{sensor} = 11 W.m^{-1}.K^{-1}, denstity (6), ρ_{sensor} = 5785 kg/m^3, and heat capacity (5), cp_{sensor} = 688.5 J.kg^{-1}.K^{-1}, of the sheath, assuming that the two materials are equally represented, as a first approximation:

$$k_{sensor} = \frac{1}{\frac{1}{k_{SS}} + \frac{1}{k_{MgO}}} \quad (4)$$

$$\rho_{sensor} = \frac{1}{2}\left(\rho_{SS} + \rho_{MgO}\right) \quad (5)$$

$$c_{P\,sensor} = \frac{1}{2}\left(c_{P_{SS}} + c_{P_{MgO}}\right) \quad (6)$$

The Biot number in the worst-case scenario (Ø 4.5 mm) in the flow condition of the reference case described next section is then 0.16 < 1.

The time constant, τ, is then expressed as per (7):

$$\tau = \frac{\rho_{sensor} V_{sensor} c_{p_{sensor}}}{h_{CO_2} A_{sensor}} \quad (7)$$

Taking 3 times the value of τ gives us an approximation of the theoretical time response at 63 % within the test tube in the reference conditions for each sensor and be compared with the manufacturer and measured ones in water in Table 2.

In addition, all sensors received a 3-points calibration (0 °C, ambient and 100 °C) against the platinum RTD before being installed on the test tube.

Table 2: Selected probes' specifications

Sen-sor type	Ø (mm)	Manufac-turer time response (s)	Manufact. uncertainty (°C)	Meas. time resp. (s)	Theor etical time resp. (s)
Pt100	3	Not given	Not given	2.1	
K	0.75	0.09	1.5	0.3	0.59
	1.5	0.3		0.5	1.18
	3	0.9		0.8	2.36
	4.5	1.4		1.0	3.54
T	1.5	0.3		0.6	1.18

It is to be noted that the data acquisition system – a mix analogue, digital and sensor measurements device equipped with a high-density thermocouple module – used has an accuracy of 50 ppm per sample rate and between ±0.02 °C ±0.25 °C on the

DOI: 10.17185/duepublico/77283

temperature measurement depending on the acquisition mode. Measurements have been done with an acquisition frequency of 40 Hz.

MEASUREMENT TEST CONDITIONS

The measurements provided in this paper, for the test tube, have been taken during the start-up of the rig going from no CO_2 circulation to established regimes. From a set of five tests, a reference case scenario is detailed below to describe the flow of CO_2 within the tube when the steady regime is achieved. In this reference case, CO_2 state variables are: T = 77.9 °C and P = 6.4 MPa and thermodynamic properties, calculated from the National Institute of Standards and Technology database [20], are gathered in Table 3 along with the reference mass flow of CO_2 and tube dimensions.

Table 3: CO_2 and tube properties

Density	$\boldsymbol{\rho_{CO_2}} = 120.97$ kg/m^3
Kinematic viscosity	$\nu = 1.58\times10^{-7}$ m^2/s
Thermal conductivity	$k = 26.12\times10^{-3}$ W/m.K
Prandtl number	$Pr = 0.97$
CO_2 mass flow	$\dot{m}_{CO_2} = 0.34$ kg/s
Tube internal diameter	$D = 26.18\times10^{-3}$ m
Tube thickness	$e = 1.2\times10^{-3}$ m
Test section length	$L = 5\times10^{-1}$ m

From these data, it is then possible to calculate the Reynolds number of the flow going through the tube using the inner diameter with (8)

$$Re_D = \frac{uD}{\nu} \tag{8}$$

With a CO_2 velocity of 5.20 m/s within the section of the tube, a Reynolds number of 8.6×10^5 is reached for our reference case confirming that the flow is fully turbulent in the test section.

To evaluate the heat transfer within the tube we are using the Dittus-Boelter correlation (9) as the Reynolds Number is above 10^4, the Prandtl number is between 0.7 and 160 and the test section aspect ratio (L/D) is superior to 10 [13].

$$Nu_D = 0.023 Re_D^{4/5} Pr^n \tag{9}$$

With n = 0.4 as the fluid is mainly heated during the experiments, we obtain a Nusselt number of 1269.6 which allows us to evaluate the heat transfer coefficient within the tube (10), h_{CO_2}:

$$h_{CO_2} = \frac{Nu_D k}{D} \tag{10}$$

The heat transfer coefficient in the test section is close to 1.27×10^3 W/m^{2}K which is around 2 orders of magnitude above the typical heat transfer coefficient in our standard laboratory room with free air flow (typically 2.5 to 25 [14]).

To generate a less severe change of temperature in the test tube, an additional scenario was generated. The stream properties in the test tube varied between conditions named state 1 and state 2 (presented in Table 4). This was achieved by bypassing the rig's gas cooler and using a Printed Circuit Heat Exchanger (PCHE) connected to a water-cooling circulation (see 'Loop 2' in Figure 4). This sudden change of boundary conditions at the sink level was enough to cause a variation of 9 kW of heat rejection, allowing to evaluate temperature variations in the test tube.

Table 4: State 1 and 2 flow conditions.

	State 1	**State 2**
Temperature (°C)	110	113
Pressure (MPa)	7.10	7.45
Density, $\boldsymbol{\rho_{CO_2}}$, (kg/m^3)	116.13	123.21
Kinematic viscosity, $\boldsymbol{\nu}$, (m^2/s)	1.77×10^{-7}	1.70×10^{-7}
Thermal conductivity, k, W/m.K	28.17×10^{-3}	28.76×10^{-3}
Prandtl number, Pr	0.90	0.91
CO_2 mass flow, $\boldsymbol{\dot{m}_{CO_2}}$, kg/s	0.19	0.19
Reynolds number, Re_D	4.5×10^5	4.4×10^5
Nusselt number, Nu	732.1	726.0
Heat transfer coefficient, $\boldsymbol{h_{CO_2}}$, (W/m^{2}K)	7.88×10^2	7.98×10^2

RESULTS

The first test to be conducted was to follow the temperature transition of the different sensors from an inactive state to the reference case described above at the compressor discharge, see Figure 6. These signals give us a reference for the temperature time evolution of typical uses of the rig detailed in this paper. This elevation of temperature corresponds to the pressure build-up first with one compressor between 70 s and 160 s where the second compressor enters into action, which causes the drop in temperature around 160 s. Despite the delay observed, all the sensors follow the same trend with a certain delay depending on the sensor itself and its location.

A first observation to be drawn is that despite the different time responses, the configuration of the installation of the probe appears to have a major impact. As could be expected, the fastest probes to react are the two directly inserted into the tube type T "in line" in Figure 6. followed by the RTD 1.6 s later. Then with a delay of 2.8 s the 3 mm K-type thermocouple in the thermowell

DOI: 10.17185/duepublico/77283

and the 0.75 mm at the surface of the tube start to measure a temperature rise. A delay that can be explained by the additional inertia induced by the wall of the thermowell and the pipe. The temperature rise is detected by the ring thermocouple 7.1 s after the first one (T-type thermocouple) due, in addition to the pipe wall's thermal inertia, to the convective heat exchanges within the room, highlights the expected necessity of thermal lagging on pipes around surface sensors.

This reference experiment gives us a first hint concerning the typical time evolution of the temperature within the tube. As a matter of fact, among the two probes to react first are the two directly in contact with the flow, as stated above, there is the RTD with the highest measured time response. Based on this observation we can estimate that this time evolution is above the 2.1 s time response of the RTD.

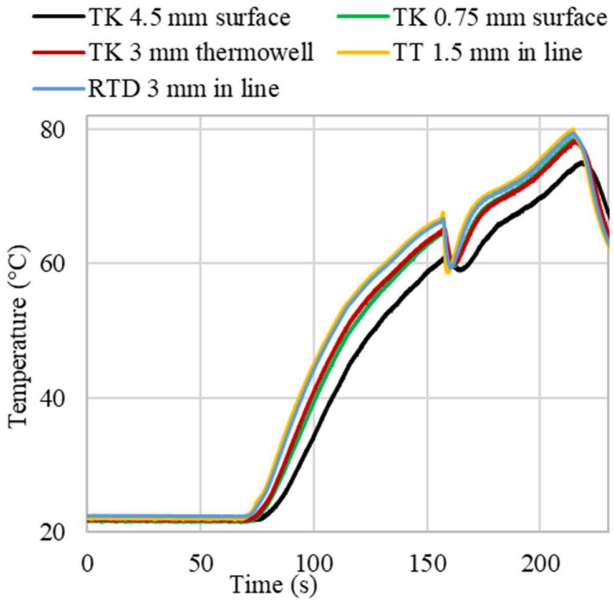

Figure 6: Typical temperature rise within the test tube from rest to the reference case of the cycle.

The results plotted in Figure 7 represent the temperature evolution of CO_2 when the system is stabilised around the condition of the reference case scenario described above. This illustrates how uneasy it is to get a fully steady state (at least in temperature) depending on the system, as the capacity of the different equipment, like the compressor, keeps adjusting to maintain the different setpoints. With these results, we notice that the three 'levels' of temperature highlighted in Figure 6 are maintained: the two sensors directly in line, TT 1.5 mm and RTD 3 mm, which keep running ahead of TK 0.75 mm at the surface and TK 3 mm in the thermowell with a temperature difference from 2 to 5 °C, and a difference between 6 and 12 °C with the TK 4.5 mm mounted on the adjustable ring.

This shows how different time responses can affect transient regimes as well as steady states. Indeed, as the different components of the rig are equipped with modulating devices and regulated via PI and PID, it is most likely that the levels of temperature and pressure never reach a smooth line but keep adjusting. Slow time responses could then introduce delays which will alter the accuracy of the temperature measurement reaching a couple of degrees. The difference with TK 4.5 mm is also most likely due to the effect of the natural convection within the test room. This could explain why the temperature never reaches the same level as the other 4.

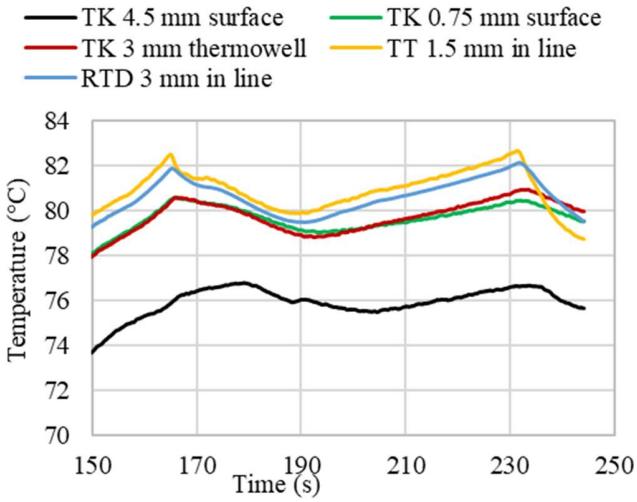

Figure 7: Temperature of CO_2 when a quasi-steady state is achieved

The second test concerns a sudden change of heat load at the sink level of the cycle from state 1 conditions to state 2 conditions (Table 4) from 25 s to around 127 s and back to state 1 from this time. This leads to a variation in the CO_2 high-pressure which comes along with an elevation or a reduction of the temperature within the test tube, see Figure 8.

A first qualitative remark is that during the rise in temperature, as no steady regime is reached, TK 0.75 mm at the surface (in green) and TK 3 mm in the thermowell (in red) never achieve the temperature of the inline RTD 3 mm (in blue) and TT 1.5 mm (in yellow) with a consistent temperature difference of 0.4 °C. However, during the step down to the lower pressure and lower temperature conditions of stage 1, the temperature, measured by the two sensors in line, drops quicker than the other two reducing the relative error between these four sensors to 0.05 °C. This means that, depending on the transition direction, if the temperature is increasing or decreasing the bias in the measurement will be higher or lower and it will not be straightforward to correct the temperature during the different transient scenarios.

DOI: 10.17185/duepublico/77283

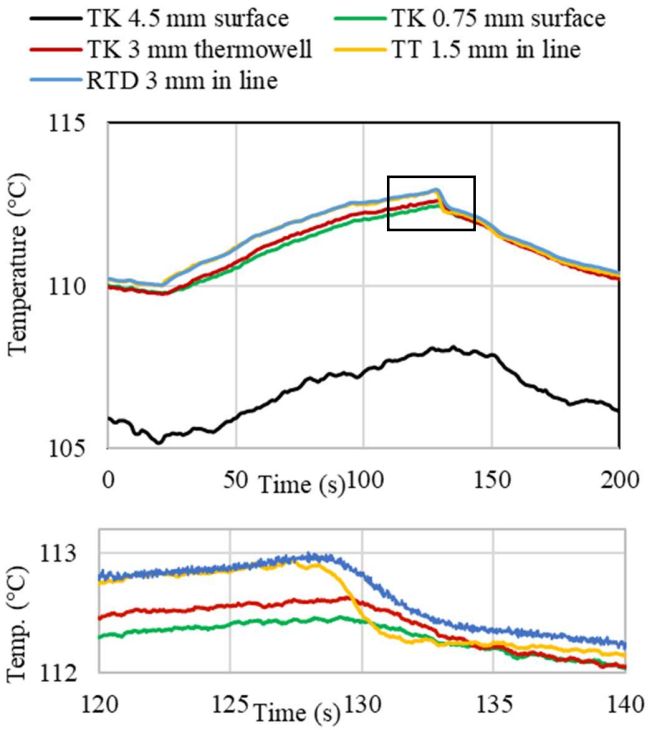

Figure 8: Temperature of CO_2 from test tube sensors during sudden flow changes between state 1 and state 2 (top) and closeup between 120 and 140 s (bottom).

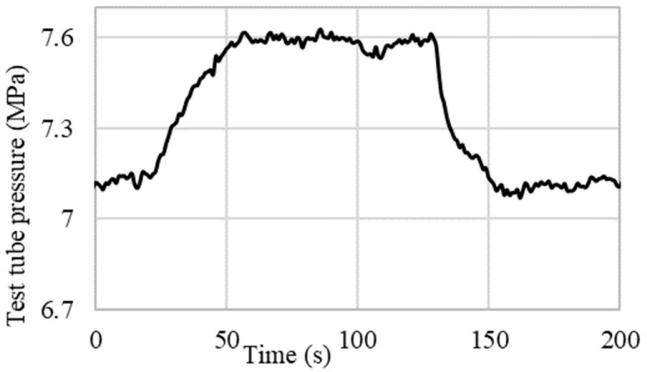

Figure 9: Measured pressure within the test tube.

The next question that can be asked is to what extent these temperature differences have an impact on calculated properties like the density or the specific enthalpy. To obtain these quantities we used the NIST database [20] considering the temperature acquired by 5 sensors of the test tube and the pressure measured during the test given in Figure 9. Calculated density and specific enthalpy are then plotted in Figure 10 and Figure 11.

To be compared, the reference properties are calculated using the temperature measured via the RTD which is supposed to have the best accuracy. Due to its interaction with the ambient ai, TK 4.5 mm leads to property calculation with the highest relative error (1 % for the enthalpy and 2.2 % for the density). For the 4 other sensors, the relative error stays below 0.2 % for the calculation of the specific enthalpy and below 0.4 % for the calculation of the density.

However, the accuracy level of the sensors should be approached with more care when investigating critical conditions as CO_2 properties can rapidly change around the critical point [15] and [16].

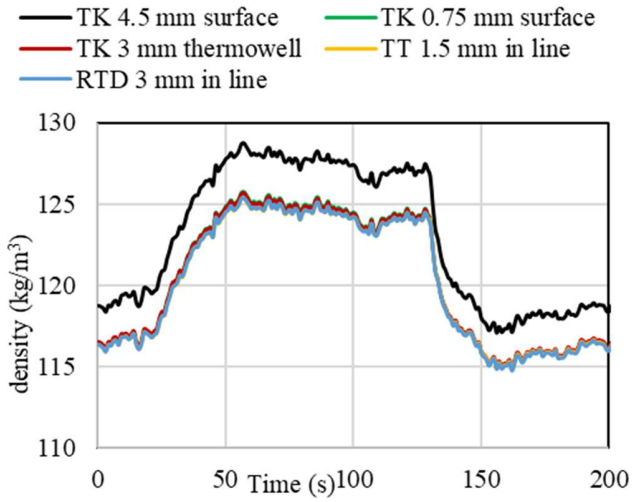

Figure 10: Calculated density of CO_2 from measurements of pressure and temperatures using the NIST database [20].

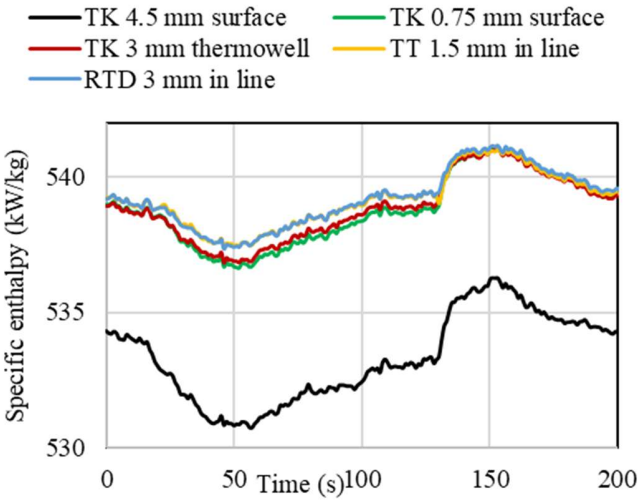

Figure 11: Calculated specific enthalpy of CO_2 from measurements of pressure and temperatures using the NIST database [20].

DOI: 10.17185/duepublico/77283

CONCLUSION

Although finding the best compromise between accuracy for performance analysis, or fast response when transient operations need to be monitored in real-time is not an easy task, the results gathered in Table 5 have the purpose to give an informed review of commonly used sensors to acquire temperature on our rig using CO_2 in a transcritical state as a working fluid.

It has been shown that, at least away from the critical point, the accuracy of the measurement implies an error on the calculation of thermodynamic properties between 0.4 and 2.2 % error for the density and 0.2 and 1 % for the enthalpy. In addition, it has been demonstrated that in the case of interaction between different regulations causing low-frequency oscillations of the steady state, slow time response sensors may introduce additional inaccuracy due to their delay to react. This makes it then trickier to provide a compensation factor to correct the measurement. To return to the introduction example, the question of keeping the compressor inlet within ± 1 °F (± 1.8 °C) becomes then very real and this additional inaccuracy turns out to be an issue to consider with care. It, thus, requires complementary measurements varying the levels of pressure and temperature to provide a complete study of the functioning conditions of the compressor.

Table 5: Summary of temperature sensors comparison results.

Sensor	Location	Δt from ref (s)	ΔT from ref (°C)
Pt 100 3 mm	In-line	1.6	Ref
TT 1.5 mm	In-line	Ref	0.5
TK 3 mm	Thermowell	2.8	2 to 5
TK 0.75 mm	Surface	2.8	2 to 5
TK 4.5 mm	Surface	7.1	6 to 12

Finally, the question of the maintenance of the sensor can be a critical parameter while selecting the right balance between a fast response or accuracy and a fast response sensor at a surface of a pipe may be advantageous compared to slow response sensor in-line as the replacement of the probe may require stopping the rig for depressurization, sensor replacement, vacuum and CO_2 refill of the pipe section.

NOMENCLATURE

A_{sensor}	Sensor surface (m^2)
D	Test tube diameter (m)
e	Test tube wall thickness (m)
h	Heat transfer coefficient ($W.K^{-1}.m^{-2}$)
k	Thermal conductivity ($W.K^{-1}.m^{-1}$)
L	Test tube length (m)
L_c	Characteristic length, $L_c = \frac{V_{sensor}}{A_{sensor}}$ (m)
$\dot{m}$	Mass flow (kg/s)
Nu	Nusselt number (-)
NIST	National Institute of Standards and Technology
P	Relative pressure (MPa)
ppm	Part per million
Pr	Prandtl number (-)
PCHE	Printed Circuit Heat Exchanger
RTD	Resistance Temperature Detector
T	Temperature (°C)
Ti	Initial temperature (°C)
TK	Thermocouple type K
TT	Thermocouple type T
T_∞	Final temperature (°C)
u	Velocity (m/s)
V_{sensor}	Sensor volume (m^3)
Δt	Time difference (s)
ΔT	Temperature difference (°C)
ν	Kinematic viscosity (m^2/s)
ρ	Density (kg/m^3)
θ	Dimensionless temperature (-)

ACKNOWLEDGEMENTS

This research has received funding from Innovate UK under project reference 113263. The authors are grateful to Rolls-Royce plc for its support during the project.

REFERENCES

[1] Pasch, J., Conboy, T., Fleming, D., Rochau, G. (2012). Supercritical CO2 Recompression Brayton Cycle: Completed Assembly Description. SANDIA Report SAND2012-9546. October 2012, Albuquerque, New Mexico and Livermore, California, USA.

[2] Hexemer, M. J. Hoang, H. Y., Rahner, K. D., Siebert, B. W., Wahl, G. D. (2009). Integrated Systems Test (IST) S-CO2 Brayton Loop Transient Model Description and Initial Results Proceedings of S-CO2 Power Cycle Symposium 2009, RPI, Troy, NY, USA, April 29-30, 2009.

[3] Baik, S., Gu Kim, S., Jun Bae, S., Ahn, Y., Lee, J., Lee, J. I. (2015). Preliminary experimental study of precooler in supercritical CO2 Brayton Cycle. Proceedings of ASME Turbo Expo 2014: Turbomachinery Technical Conference and Exposition, Montreal, Canada, June 15-19, 2015. Paper GT2015-42915.

[4] Anselmi, E., Zachos, P., Collins, R., Hassan, M. (2016). Development of an experimental S-CO2 loop for bottoming cycle applications. 1st European Seminar on SCO2 Power Systems, Vienna, Austria, 29-30 September 2016.

[5] Clementoni, E. M., Cox, T. R. L. (2014). Comparison of Carbon Dioxide property measurements for an operating supercritical Brayton Cycle to the REFPROP physical properties database. Proceedings of ASME Turbo Expo 2014: Turbomachinery Technical Conference and Exposition, Dusseldorf, Germany, June 16-20, 2014. Paper GT2014-25338.

[6] Wahl, A., Mertz, R., Laurien, E., Straflinger, J. (2019). Experimental investigation of heat transfer and pressure drop in tubes to cool CO2 near the critical point. 3rd European supercritical CO2 Conference, Paris, France, September 29-10, 2019. Paper 2019-sCO2.eu-131.

DOI: 10.17185/duepublico/77283

[7] Hacks, A. J., Vojacek, A., Dohmen, H. J., Brillert, D. (2018). Experimental investigation of the sCO2-HeRo compressor. 2nd European supercritical CO2 Conference, Essen, Germany, August 30-31, 2018. Paper 2018-sCO2.eu-115.
[8] Vojacek, A., Melichar, T., Hajek, P., Doubek, F., Hoppe, T. (2019). Experimental investigation and simulations of the control system in supercritical CO2 loop. 3rd European supercritical CO2 Conference, Paris, France, September 29-10, 2019. Paper 2019-sCO2.eu-148.
[9] Clementoni, E. M., Cox, T. R. L., King, M. A., Rahner, K. D. (2017). Transient Power Operation of a Supercritical Carbon Dioxide Brayton Cycle. Proceedings of ASME Turbo Expo 2017: Turbomachinery Technical Conference and Exposition, Charlotte, NC, USA, June 26-30, 2017. Paper GT2017-63056.
[10] Moore, J. (2017). Chapter 9: Auxiliary Equipment in Fundamentals and applications of supercritical carbon dioxide (sCO2) based power cycles, from Brun, K., Friedman, P., Dennis, R. Woodhead Publishing, Elsevier Ltd. UK. ISBN 978-0-08-100805-8.
[11] Rapp, L. (2022). Experimental testing of a 1MW SCO2 Turbocompressor. The 7th International Supercritical CO2 Power Cycles Symposium. San Antonio, Texas, USA. February 21-24, 2022. Paper #32.
[12] Anselmi, E., Bunce, I., Pachidis, V. (2019). An overview of initial operating experience with the closed-loop sCO2 test facility at Cranfield University. Proceedings of ASME Turbo Expo 2019, Phoenix, Arizona, USA, June 17-21, 2019, ASME Paper No. GT2019-91391.
[13] Mills, A. F. (1992). Heat Transfer, United States, Los Angeles.
[14] Kosky, P., Balmer, R., Keat, W., Wise, G. (2013). Exploring Engineering.
[15] Polikhronidi, N., Batyrova, R., Aliev, A., Abdulagatov I. (2019). Supercritical CO_2: Properties and Technological Applications - A Review. Journal of Thermal Science, 28, pages 394–430.
[16] Abdulagatov, I. M., Skripov, P. V. (2021). Thermodynamic and Transport Properties of Supercritical Fluids. Part 2: Review of Transport Properties. Russian Journal of Physical Chemistry B volume 15, pages 1171–1188.
[17] Mortzheim, J., Hofer, D., Priebe, S., McClung, A., Moore, J. J., Cich, S. (2021). Challenges with measuring supercritical CO2 compressor performance when approaching the liquid-vapor dome. Proceedings of ASME Turbo Expo 2021: Turbomachinery Technical Conference and Exposition, Virtual, Online, June 7-11, 2021. Paper GT2021-59527.
[18] Marchionni, M. (2021). PhD Thesis, page 88
[19] Illyés, V., Morosini, E., Doninelli, M., David, P.-L., Guerif, X., Werner, A., Di Marcoberardino, G., Manzolini, G. (2022). Design of an air-cooled condenser for co2-based mixtures: model development, validation and heat exchange gain with internal microfins. Proceedings of ASME Turbo Expo 2022, June 13-17 2022. Paper GT2022-82438.
[19] Incropera, F. P., DeWitt, D. P., Bergman, T. L., Lavine, S. L. (2006). Fundamental of Heat and Mass Transfer.
[20] Lemmon, E. W., Bell, I. H., Huber, M. L., Mc Linden, M.O. (2018). NIST Standard Reference Database 23: Reference Fluid Thermodynamic and Transport Properties-REFPROP, Version 10.0, National Institute of Standards and Technology, Standard Reference Data Program, Gaithersburg.

 DOI: 10.17185/duepublico/77283

DOI: 10.17185/duepublico/77283
URN: urn:nbn:de:hbz:465-20230427-122017-6